Pokorný et al. *NPG Asia Materials* (2021) 13:66
https://doi.org/10.1038/s41427-021-00332-w

NPG Asia Materials

ARTICLE Open Access

# Gd-admixed (Lu,Gd)$AlO_3$ single crystals: breakthrough in heavy perovskite scintillators

Martin Pokorný[1,2], Vladimir Babin[1], Alena Beitlerová[1], Karel Jurek[1], Jan Polák[3], Jindřich Houžvička[3], Dalibor Pánek[4], Tomáš Parkman[4], Vojtěch Vaněček[1,4] and Martin Nikl[1]

**Abstract**

We report a breakthrough concept for a bulk single crystal as a heavy aluminum perovskite scintillator, where due to bandgap engineering by a balanced Gd admixture in a Lu cation sublattice, the scintillation performance dramatically increases. In an optimized composition of (Lu, Gd)$AlO_3$:Ce (LuGdAP:Ce), the light yield approaches 21,000 phot/MeV, which is close to that of classical but much less dense YAP:Ce and 50% higher than the best LuYAP:Ce reported in the literature. Moreover, contrary to LuYAP:Ce, the LuGdAP host maintains a high effective atomic number close to that of LuAP:Ce ($Z_{eff} = 64.9$), which is comparable to commercial LSO:Ce. An enormous decrease in afterglow on the millisecond time scale and acceleration in the rise time of the scintillation response further increase the application potential of the LuGdAP host. The related acceleration of the transfer stage in the scintillation mechanism due to diminishing electron trap depths is proven by thermally stimulated luminescence (TSL). Furthermore, we quantitatively characterize and model the energy transfer processes that are responsible for the change in the photoluminescence and scintillation decay kinetics of $Ce^{3+}$ in the LuGdAP matrix. Such an innovative (Lu, Gd)AP:Ce scintillator will become competitive for use in applications that require heavy, fast, and high light yield bulk scintillators.

## Introduction

Single crystal oxide-based scintillation materials are widely used in practical applications due to their mechanical and chemical stability and high performance[1,2]. The green-yellow emitting YAG:Ce ($Y_3Al_5O_{12}$ doped with $Ce^{3+}$) single crystal has been one of the best-known scintillator and phosphor materials since the 1970s[3,4]. Due to its low density and effective atomic number ($Z_{eff}$), the R&D focus has oriented toward its heavy analog $Lu_3Al_5O_{12}$:Ce (LuAG:Ce) and finally to multicomponent garnets based on the general formula $(Lu,Y,Gd)_3(Ga,Al)_5O_{12}$:Ce (see the review)[5]. Based on a tailored modification of the electronic band structure, so-called "bandgap engineering", such multicomponent compositions may offer superior scintillation performance compared to their simpler counterparts. Namely, a significant decrease in the afterglow, faster scintillation decay, and higher light yield have been demonstrated. All these characteristics are shaped by the energy transfer and charge trapping in the transfer stage of the scintillation mechanism (i.e., determined by the matrix composition and defects) or even by the luminescent center itself.

The flexible composition of the $(Lu,Y,Gd)_3(Ga,Al)_5O_{12}$:Ce garnet crystal matrix enables extended composition tailoring, which positively affects timing and efficiency-related scintillation characteristics[6–9]. This effect can be further enhanced by the stabilization of the $Ce^{4+}$ center due to the stable divalent ion codoping reported in 2014[10]. The same bandgap engineering strategy was also successfully applied in cerium-doped orthosilicates of the general formula $(Lu,Y,Gd)_2SiO_5$:Ce[11,12]. The maximized light yield was achieved with $(Lu_{0.6}Gd_{0.4})_2SiO_5$; additionally, $Lu_{1.8}Y_{0.2}SiO_5$ (LYSO) was easier to grow than $Lu_2SiO_5$ LSO. The positive effect of $Ce^{4+}$ stabilization by

Correspondence: Martin Nikl (nikl@fzu.cz)
[1]Institute of Physics of the Czech Academy of Sciences, Cukrovarnická 10/112, 162 00 Prague 6, Czech Republic
[2]Faculty of Mathematics and Physics, Charles University in Prague, Ke Karlovu 3, 121 16 Prague 2, Czech Republic
Full list of author information is available at the end of the article

divalent ion doping on the scintillation characteristics of LYSO:Ce was explained in 2013[13]. It is also worth mentioning bandgap engineering in pyrosilicates, especially in La-admixed $Gd_2Si_2O_7$:Ce, where the La-admixture has been primarily used to stabilize crystal growth[14]. All of these multicomponent crystal growth strategies are enabled by the existence of solid solutions that initially consist of binary constituents, which enable congruent crystal growth and are driven by the idea of further optimizing a material (higher light yield, faster decay, higher X-ray (gamma) attenuation, better energy resolution, etc.).

However, such a systematic combination of research has not yet been done with bulk perovskite scintillators that contain analogous-to-garnet chemical elements in another stoichiometry (Y,Gd,Lu)(Al,Ga)$O_3$:Ce. Furthermore, individual attempts that have been reported thus far have not provided satisfactory results in the search for heavy aluminum perovskite scintillators to satisfy the need for high-density analogs of classical, bright, but low density and $Z_{eff}$ $YAlO_3$:Ce (YAP:Ce) single crystals. In this search, the bulk single crystal of $LuAlO_3$:Ce (LuAP:Ce) became of topical interest in the mid-1990s. The $Ce^{3+}$ center in the LuAP host shows emission with a maximum at ~360 nm, photoluminescence (PL) decay time of ~18 ns[15–17], and a typical light yield value from 7000–9000 photons/MeV[18] that can shift up to 12,000 photons/MeV[16]. Such values are highly inferior to commercial YAP:Ce with an LY slightly above 20,000 photons/MeV. Because of the extremely unstable growth of the LuAP phase, an admixture of yttrium was adopted (up to 30 at.%) for large crystal growth; however, no noticeable enhancement in scintillation performance was observed[18,19]. In pure LuAP:Ce, the scintillation decay is composed of several well-resolved components, some of which vary with temperature[20], which is certainly an effect of electron trapping in the transfer stage of the scintillation mechanism. Indeed, thermally stimulated luminescence (TSL) measurements in ref. [20] revealed the most intense peak at 183 K with a calculated trap depth of 0.49 eV and a detrapping time of 140 μs at RT. The relation between the TSL characteristics over a wide temperature range above RT and the temperature dependence of the light yield value in LuAP:Ce were also further discussed[21]. The preparation of a $GdAlO_3$ single crystal (with more stable crystal growth) also did not provide satisfactory results regarding its scintillation performance. One of the reasons is that due to the weaker crystal field in the perovskite host, the emission peak of $Ce^{3+}$ undergoes a high-energy shift to 360–370 nm, and the reverse energy transfer $Ce^{3+}$ ($5d_1$) → $Gd^{3+}$ ($^6P_{3/2,\ 5/2,\ 7/2}$[22]) becomes possible. This behavior dramatically deteriorates the scintillation performance of GdAP[23]. The scintillation decay kinetics of $GdAlO_3$:Ce also change with different Ce concentrations in the range of 0.02–0.75 mol%, which is ascribed to the $Gd^{3+}$ → $Ce^{3+}$ energy transfer[24]. In the case of small, low-quality bulk LuGdAP:Ce crystals, the $Ce^{3+}$ → $Gd^{3+}$, $(Gd^{3+} \rightarrow Gd^{3+})_n$ and $Gd^{3+}$ → $Ce^{3+}$ energy transfers have already been identified and briefly described[25] with just a qualitative interpretation: The energy migration enabled by the Gd sublattice results in a slow secondary decay component (delayed luminescence) of $Ce^{3+}$ emission, as well as an acceleration of the primary component of Ce decay due to energy transfer out of the $5d_1$ state toward a nearby positioned $Gd^{3+}$ cation. More recently, the trapping and detrapping processes of electrons and holes in $GdAlO_3$:$Ce^{3+}$, $Ln^{3+}$ (Ln = Er, Nd, Ho, Dy, and Tm) were studied[26], in which the $Ln^{3+}$ codopant was the electron trapping center and $Ce^{3+}$ was the hole trapping and recombination center. The authors also theoretically proved that the admixture of La could be used to modify the valence band edge and influence the hole trap depths.

More systematic experimental research on such multicomponent perovskite materials in the form of single-crystal films prepared by liquid phase epitaxy (LPE) has recently restarted because of their potential for high-resolution 2D imaging[27]. However, such a technology is limited to film thicknesses up to several tens of micrometers; thus, this technology cannot provide bulk optical elements that are readily available from bulk crystal growth technologies. In LPE-grown YGdAP:Ce with a Gd concentration >20%, the $Gd^{3+}$ emission line at 311 nm diminishes due to concentration quenching and/or the $Gd^{3+}$ → $Ce^{3+}$ energy transfer[28]. Moreover, the YAP host exciton emission (the broad peak at 302 nm)[29] is quenched at high Gd dopant concentrations due to the efficient energy transfer from the host to $Gd^{3+}$. For these (Y,Gd)AP:Ce LPE layers, the energy transfer from $Ce^{3+}$ to $Gd^{3+}$ is successfully described by the Inokuti–Hirayama model[30], in which both transitions demonstrate dipole character[31]. Strong acceleration of the primary $Ce^{3+}$ decay component is observed, and a slow (τ = 60–250 ns) decay component appears with increasing Gd content.

Notably, a recent theoretical study, which used density functional theory, focused on the possibility of eliminating the effects of radiation-induced damage by bandgap engineering the LuAP:Ce scintillator[32]. The above study examined the role of the Ga admixture at the Al site and found that $LuGaO_3$ should have a bandgap that was more than 2 eV smaller than that of $LuAlO_3$. Then, the lowered conduction band edge in Lu(Al,Ga)$O_3$:Ce enveloped the defect gap states, eliminating their potential negative impact on scintillation performance. Therefore, ref. [32] provides a direct theoretical concept for how band-edge engineering could be applied to rare-earth-doped LuAP scintillators, and such a study calls for experimental verification.

In this paper, we present the results of measurements performed on a unique set of bulk LuGdAP:Ce single

crystals prepared by the Czochralski method, where the Gd-to-Lu ratio was varied from 0 to 1.5. Their PL characteristics were measured, focusing on two main effects: (i) nonradiative energy transfer from the $Ce^{3+}$ center toward $Gd^{3+}$, resulting in the acceleration of the PL decay kinetics of the $Ce^{3+}$ center and (ii) the subsequent reverse energy transfer $Gd^{3+} \rightarrow Ce^{3+}$, resulting in delayed radiative recombination at $Ce^{3+}$ which visualizes the energy migration within the Gd sublattice. The measured TSL glow curves proved the decrease in the depth of the electron traps, which explained diminishing their negative effect on the scintillation properties. Most importantly, the practical aspects, including the afterglow, scintillation rise, and decay on an extended dynamic time scale and light yield, were measured. All these results clearly showed that the bandgap engineering strategy and host optimization by the balanced Gd admixture in LuAP:Ce significantly accelerated the transfer of excitation energy toward the luminescent centers, sped up all the scintillation mechanism, and increased the light yield. Therefore, this strategy opens a breakthrough pathway for bulk heavy aluminum perovskite scintillators with a high potential for use in practical applications.

## Measurement methods

The absorption spectra were recorded by a Shimadzu 3101 PC spectrometer (Shimadzu). A custom-made 5000 M Horiba Jobin Yvon spectrofluorimeter equipped with a TBX-04 photon-counting detector was used for both the PL and radioluminescence (RL) measurements. Excitation was performed by an X-ray tube (Seifert GmbH) operated at 40 kV (RL) or a laser-driven plasma light source (Energetiq) (PL), and all spectra were corrected for distortions caused by the apparatus. The PL decays were measured with nanoLED 310 nm (Horiba, nominal pulse duration of 1.2 ns) excitation, and the emission was detected in the spectral range of 373–377 nm, where the $Ce^{3+}$ emission dominated and no $Gd^{3+}$ emission was present. The apparatus was operated in the time-correlated single-photon counting mode with a temporal resolution well below 1 ns (FWHM of the measured instrument response was 1.2 ns). Convolution of the instrument response with model function is used during the fitting procedure in each iteration step.

For the ultrahigh temporal resolution needed to measure the scintillation rise time, the samples were excited by a picosecond pulsing X-ray source (40 kV) from Hamamatsu. The signal was detected by a hybrid picosecond photon detector HPPD-860 and Fluorohub unit from Horiba Scientific. The curves were analyzed in SpectraSolve software (Ames Photonics) using a three-exponential model function, again with the convolution of the instrumental response. The instrumental response function FWHM was ~76 ps.

For the TSL study, all the samples were measured under the same conditions. The sample was glued with silver paint to the cold finger of a cryostat (Oxford Instruments) and fixed by a copper mask. At 77 K, the sample was irradiated for 10 min by a 40 kV/15 mA X-ray tube with a W target (Seifert GmbH). After irradiation, the sample was kept at a low temperature for 30 min to allow the afterglow to fade. Finally, the TSL run was initiated in the range of 77–500 K with a linear heating rate of 0.1 K/s (6 K/min).

To monitor the scintillation decay in ultrabroad time intervals, a nanosecond soft X-ray (FWHM of ~5 ns), 0.4 keV pulsed plasma excitation source, and Hamamatsu R7056 photomultiplier in the current analog mode with an Agilent DSO7104 oscilloscope were used in the detection chain[33]. This setup offered an excellent S/N ratio together with the ability to record the decay curve over time across six orders of magnitude (1 ns up to 1 ms). Again, a convolution of the multiexponential function with the measured instrument response was used for the fitting procedure.

## Experimental results and discussion

### Crystal growth

All crystals were grown by the Czochralski method in an inductive furnace from the CRYTUR company (Turnov, Czech Republic) under analogous conditions as in Photonics Materials, Ltd.[18]. Five crystals with different Gd contents were grown. The concentration of Gd was increasing from zero in $LuAlO_3$ (sample Gd0) up to $Lu_{0.39}Gd_{0.61}AlO_3$ (sample Gd0.61). This short notation of the samples is used throughout the text. Samples with thicknesses of ~0.64 mm and diameters of 10 mm or square shapes of 7 $mm^2 \times 7$ $mm^2$ (Fig. 1) were cut from single-crystal boules, polished on both sides, and used for the abovementioned optical, RL, and scintillation measurements. Moreover, elemental analysis (Electron Probe MicroAnalyzer, JEOL JXA-8230 with WDS detector) was performed to check the composition of the samples. It showed an increasing content of Ce with increasing Gd content, which was ascribed to a more favorable segregation coefficient of Ce in the host, similar to Gd-admixed orthosilicates[12] or garnets[5].

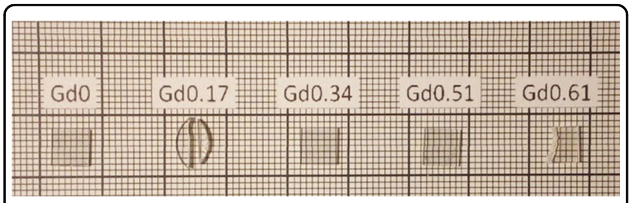


**Fig. 1 Photograph of all the samples.** Gd0.17 and Gd0.61 cracked during cutting and polishing.

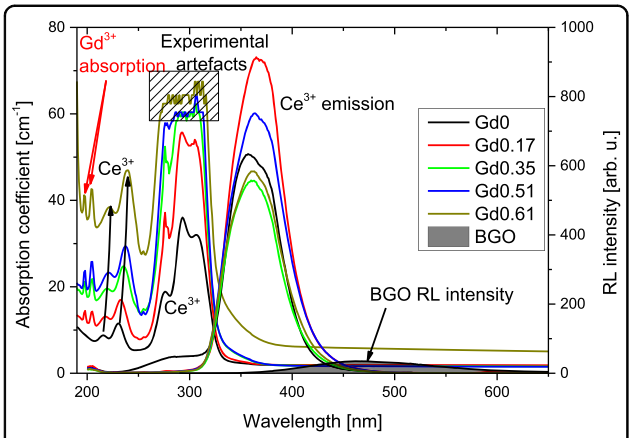


**Fig. 2 Comparison of the absorption and radioluminescence spectraof the samples.** The latter spectra are dominated by $Ce^{3+}$ emission and compared in absolute scale with BGO standard scintillator plate.

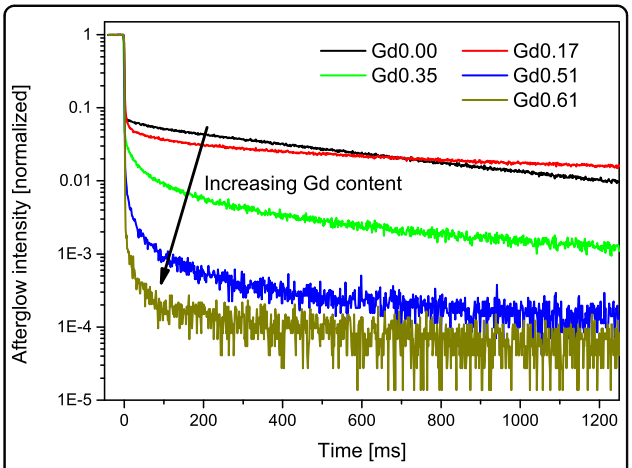


**Fig. 3 Measured afterglow profiles.** Excitation by X-rays, 40 kV, 10 mA, cut-off at t = 0 ms.

## Characterization of the optical and scintillation properties

In the measured absorption spectra, five $Ce^{3+}$ 4f → $5d_n$ ($n = 1–5$) absorption bands are clearly visible in the LuAP:Ce sample (Gd0). Their positions coincide with those reported before; see, for example, ref. [34]. The assignment of the individual absorption transitions is provided in the Supporting Information (SI), Figure S1, and Table S1, according to the theoretical study[35]. With the admixture of Gd, two additional sharp bands at 198 and 204 nm ascribed to $Gd^{3+}$ $^8S_{7/2}$ → $^6G_{7/2}$ appear[36]. Moreover, unidentified UV absorption ($\lambda < 250$ nm) is observed with Gd codoping. Another noteworthy point is that the broad host emission from 250–300 nm (self-trapped exciton or trapped hole at the $Lu_{Al}$ defect[37]), which spectrally overlaps with the $Ce^{3+}$ absorption, vanishes even at the lowest Gd concentration (Fig. 2).

The absolute value of the absorption coefficient in the broad bands from 270–320 nm could not be reliably computed for the three highest Gd-admixed 0.64 mm thick samples on our apparatus. The values were higher than 50 $cm^{-1}$; thus, the signal was lost in the noise of the apparatus.

The comparison of the afterglow profiles of the samples is shown in Fig. 3. In the samples with the highest Gd content, a very large decrease in afterglow intensity is observed, which (considering that the integral RL intensity remains the same within ±20%) suggests that the very slow afterglow components in LuAP:Ce (not detected by the light yield measurement) are transformed into faster decay components due to the incorporation of Gd in the matrix. Interestingly, in the sample with the lowest Gd content (Gd0.17), the afterglow intensity does not decrease, and its time course becomes slower, which is an interesting degradation phenomenon.

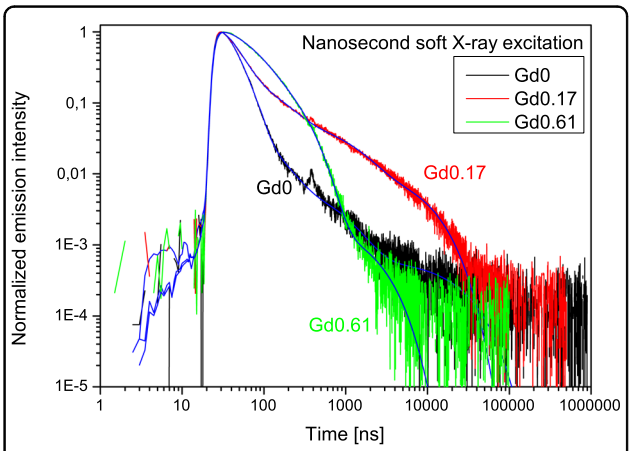


**Fig. 4 Scintillation time profiles (spectrally unresolved, excited by nanosecond soft X-ray pulse).** The sharp peak from 350–400 ns is an experimental artifact. Solid lines are the convolutions of the instrumental response and four-exponential function with the parameters in Table 1.

In the measured scintillation decays over the 1 ns–1 ms time range under soft X-ray nanosecond pulse excitation, which are shown in Fig. 4, several phenomena are worth commenting. When comparing the lowest Gd concentration with the Gd0 sample, additional components within the sub-μs–tens-of-μs time range appear. With increasing Gd content, the slowest component accelerates, and for Gd0.61, the intensity becomes lower than that of LuAP:Ce at times beyond 2 μs after excitation.

The fitting results of the scintillation decay curves in Fig. 4 are presented in Table 1. With increasing Gd content, the fastest component becomes somewhat slower (its decay time increases from 18 ns up to 44 ns for the

Gd0.61 sample). Regarding the highest Gd-codoped sample, the first component together with the second component (τ ~100–160 ns) contained 96% of all the scintillation light.

The spectrally unresolved scintillation decays of all samples under excitation by the $^{137}$Cs (662 keV) radioisotope in a time window of 0–5000 ns and their integrals are provided in the SI, Fig. S2, and Table S2. These results confirm the gradual deceleration of the fastest component with increasing Gd content until reaching Gd0.51 and the acceleration in the decay tail of Gd0.51 and Gd0.61 compared to that of the Gd-free sample; additionally, the time development of the normalized integrals of the scintillation decays are shown in Fig. S3.

Another significant positive effect on the scintillation time profile is proven using picosecond X-ray pulse excitation, Fig. 5. The scintillation rise time of LuAP:Ce is 0.76 ns, and with Gd codoping, it decreases to 0.46 ns (sample Gd0.17) and even down to 0.26 ns (sample Gd0.35). Notably, additional increases in the Gd content no longer decreases the rise time. A rise time that is as short as possible together with a fast decay time and high light yield are critically important for time-of-flight techniques in radiation detection, e.g., in the latest generation of positron emission tomography medical imaging[38].

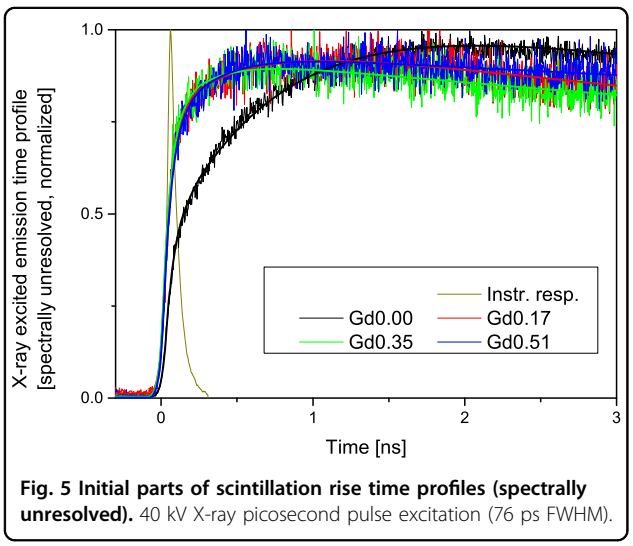


**Fig. 5 Initial parts of scintillation rise time profiles (spectrally unresolved).** 40 kV X-ray picosecond pulse excitation (76 ps FWHM).

A summary of the scintillation characteristics is provided in Table 2. With the exception of Gd0.17, all the samples show monotonic trends in their afterglow intensity and scintillation rise time values. From the light yield measurement, sample Gd0.51 appears to be the best sample because it shows the highest light yield and best energy resolution.

Sample Gd0.17 has the lowest light yield and the worst energy resolution, which is different from the trends observed in the remaining Gd-admixed samples. This points to a more complex influence of the Gd concentration on scintillation performance. We conclude that at low Gd concentrations, the Gd admixture has a rather negative impact because it drains energy from $Ce^{3+}$, but due to the diluted Gd sublattice, the energy returns back to Ce very slowly, resulting in the intense but slowest afterglow and a low light yield.

## Energy transfer processes in PL: The model

To characterize the energy transfer away from the $5d_1$ state of $Ce^{3+}$, PL decay curves (excitation by nanoLEDs at 310 nm, emission at 375 nm) were measured and analyzed. The model function is:

$$I(t) = A\times \exp\left[-\frac{t}{\tau_{\mathrm{rad}}} - a\times\left(\frac{t}{\tau_{\mathrm{rad}}}\right)^{3/s}\right] + A_2\times \exp\left(-\frac{t}{\tau_2}\right) + \text{background}, \quad (1)$$

(see the model details in the SI, in the section "Microscopic Modeling of Photoluminescence Decay") which is convoluted with the measured instrument function in each iteration step. The results of the fits are shown in Table 3 and Table S3.

In the Gd-free LuAP:Ce, the decay is monoexponential over three decades with a decay constant of $\tau_{\mathrm{rad}} = 16.8$ ns. Regarding the Gd-admixed samples, the value of the parameter $\tau_{\mathrm{rad}}$ was kept fixed, and the varied parameters were $A$, $\alpha$, $A_2$ and $\tau_2$, where $\alpha = \frac{c_A}{c_{A0}}\Gamma\left(1-\frac{3}{s}\right)$ and $A_2$ and $\tau_2$ are the amplitude and decay constants of the second

**Table 1 Summary of the decay time and intensity values from the four-exponential approximation of the scintillation response after nanosecond soft X-ray excitation.**

| | Signal amplitude | First component | | Second component | | Third component | | Fourth component | |
|---|---|---|---|---|---|---|---|---|---|
| Sample | [Volts] | τ [ns] | (I [%]) | τ [ns] | (I [%]) | τ [ns] | (I [%]) | τ [ns] | (I [%]) |
| Gd0 | 0.970 | 18.2 | (52%) | 94 | (8%) | 785 | (10%) | 25 850 | (31%) |
| Gd0.17 | 0.178 | 19.0 | (12%) | 112 | (11%) | 1 041 | (25%) | 9 003 | (52%) |
| Gd0.61 | 0.666 | 44.0 | (36%) | 163 | (60%) | 1 866 | (4%) | | |

**Table 2 Summary of the main scintillation characteristics of the samples.**

| Sample | Composition [Gd] | Composition [Ce] | Integral of RL % of BGO | LY @ 662 keV ph/MeV | En res @ 662 keV | Afterglow @ 100 ms | X-ray rise time ns | Zeff (E = 15 keV) |
|---|---|---|---|---|---|---|---|---|
| BGO | | -- | 100% | 9 000 | | | | |
| Gd0.00 | 0 | 0.0014 | 762% | 13 100 | 12% | 5.1% | 0.76 | 66.0 |
| Gd0.17 | 0.168 | 0.002 | 1 038% | 7 700 | 32% | 3.7% | 0.46 | 65.0 |
| Gd0.35 | 0.345 | 0.0028 | 643% | 14 400 | 10% | 0.86% | 0.26 | 63.9 |
| Gd0.51 | 0.508 | 0.0037 | 901% | 21 000 | 10% | 0.08% | 0.27 | 62.7 |
| Gd0.61 | 0.613 | 0.0051 | 696% | 16 800 | 17% | 0.02% | NM | 61.7 |

Effective atomic number calculation is provided in SI, part "The determination of the effective atomic number, $Z_{eff}$".
*NM* not measured.

**Table 3 Results of the photoluminescence decays fitting using the Förster–Dexter model (Eq. 1).**

| | Förster–Dexter component | | | | Second component | | |
|---|---|---|---|---|---|---|---|
| Sample | A | $\tau_{rad}$ [ns] | α | $I_1$ | $\tau_2$ [ns] | $I_2$ | $A_2$ |
| Gd0 | 1.22 | 16.81 | 0.000 | 95% | 424 | 5% | 0.002 |
| Gd0.17 | 1.23 | 16.81 | 0.092 | 94% | 77 | 6% | 0.016 |
| Gd0.35 | 1.41 | 16.81 | 0.398 | 86% | 149 | 14% | 0.019 |
| Gd0.51 | 1.45 | 16.81 | 0.668 | 61% | 215 | 39% | 0.041 |
| Gd0.61 | 1.63 | 16.81 | 1.069 | 46% | 209 | 54% | 0.063 |

A detailed description of the fitting procedure is provided in the SI.

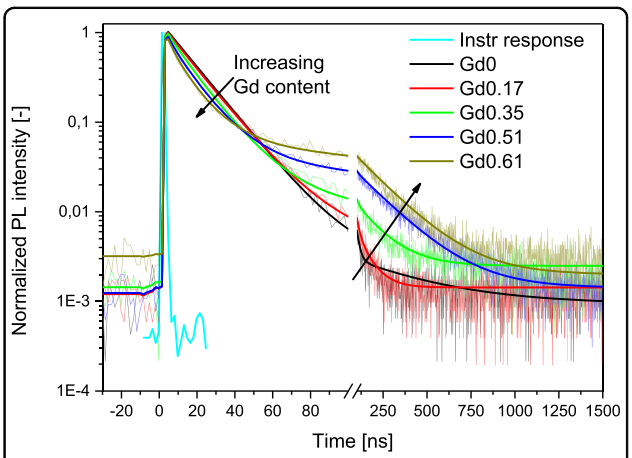


**Fig. 6 Comparison of the PL decay time profiles.** The smooth lines are convolutions of the model function (Eq. 1) and the measured instrument response (drawn in cyan in the figure).

exponential component, respectively (Eq. 1). A detailed view and description of the model function for the Gd0.51 sample is provided in the SI (Fig. S4). For all sample sets, a gradual acceleration in the primary decay component is clearly seen in Fig. 6 and Fig. S5, as well as a monotonic increase in the intensity of the slower (sub-μs) component. This is in accordance with the measured intensities of the RL spectra, which show a decrease of only ~20% for the high Gd-codoped samples with respect to the LuAP:Ce sample. Hence, the energy that is non-radiatively transferred away from the Ce $5d_1$ state is not lost but reemitted in a major way at some later time (a few hundred nanoseconds). Hence, the energy drawn away from $Ce^{3+}$ is not lost for scintillation but returns to the (same or different) $Ce^{3+}$ center and gives rise to delayed radiative recombination at the sub-microsecond time scale. Consequently, these energy transfer processes are fast enough to be covered by the standard shaping time of

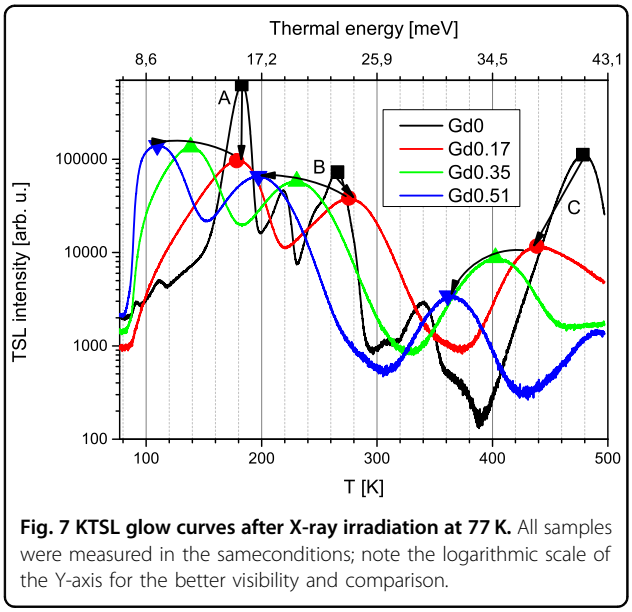


**Fig. 7 KTSL glow curves after X-ray irradiation at 77 K.** All samples were measured in the sameconditions; note the logarithmic scale of the Y-axis for the better visibility and comparison.

1 μs in the LY measurement, and no LY loss occurs. A general comparison of the 1/e decay time values for the PL, $^{137}$Cs and pulse X-ray excited decays is provided in Table S4.

To understand the change in the afterglow profiles at longer time scales, the electron trap depths were investigated by analyzing the TSL glow curves (Fig. 7).

All the TSL peaks move to lower temperatures with increasing Gd content, which is a clear indication of diminishing the depth of the related traps (peak A moves from 183 (sample Gd0) to 110 K (sample Gd0.51), peak B moves from 266 to 197 K, and peak C moves from 478 to 361 K). The position of the TSL peaks measured for pure LuAP:Ce here agrees very well with those published in earlier papers both below RT[16] and above RT[21] temperature regions after taking into account the different heating rates in the latter.

A detailed analysis of TSL glow curves below room temperature in YAP:Ce[39] and LuAP:Ce[16] was reported. These TSL curves are dominated by the peaks at 105 K (trap depth of 0.18 eV) and 182 K (trap depth of 0.51 eV), respectively. The nature of the related electron trap is probably similar taking into account the in-between temperature position of such a peak in mixed LuYAP:Ce[37], in which a set of intense peaks in the range of 100–300 K is observed. We conclude that these traps are related to the Y(Al) and Lu(Al) antisite defects in the YAP and LuAP hosts (melt-grown bulk crystals), respectively, given the similarity in their chemical composition, such as the TSL trap positioning and related luminescence characteristics of YAG:Ce and LuAG:Ce (see refs. [5,9,39,40]) and the experimental evidence of the Y(Al) antisite defects in the YAP crystal from the NMR experiment[41].

The detrapping times of the related traps in the dominant glow curve peaks mentioned above for YAP:Ce and LuAP:Ce at room temperature were calculated within 100–200 μs[16,39], which is the time window caught neither by the scintillation decay nor the afterglow measurement. It is worth noting that the detailed analysis of the PL decay curves[17] of LuAP:Ce also evidenced a trap depth of 0.14 eV without the need to measure the TSL glow curves.

In a recent theoretical paper[40], in the YAP matrix, the 4d state of the antisite defect Y(Al) (= yttrium ion at the aluminum position) was calculated to be 0.87 eV below the Y (Y) 4d state, and the Al(Y) 3 s state was 0.21 eV below the Al (Al) 3 s state. Taking into account that the thermal trap depth measured in the TSL experiment can typically be a few times lower than the calculated optical (vertical) trap depth, the experimental and theoretical values are comparable. This result also supports the abovementioned attribution of the dominant glow curve peaks at 105 K for YAP:Ce and at 183 K for LuAP:Ce to the Y(Al) and Lu(Al) antisite defect-based traps, respectively.

According to the theoretical DFT computations in ref. [32], the conduction band edge of GdAP should be lowered by ~2.5 eV compared to that of LuAP. Therefore, the decreasing edge of the conduction band should effectively cover all the mentioned shallow electron traps, provided that the positions of the traps remain unchanged. As we observe, all the TSL glow curve peaks shift toward lower temperatures (i.e., lower trap depths) with increasing Gd admixture; therefore, we confirm that the conduction band edge does approach the electron trap levels.

## Conclusions

The LuAP:Ce single crystal admixed with a balanced Gd content results in a heavy aluminum perovskite scintillator with excellent scintillation performance. The best performing composition $(Lu_{0.5}Gd_{0.5})AlO_3$:Ce has a light yield value of 21,000 phot/MeV. Compared to pure $LuAlO_3$:Ce, the $(Lu_{0.5}Gd_{0.5})AlO_3$:Ce shows a 60% increase in the light yield and a faster scintillation rise time (0.27 ns compared to 0.76 ns in LuAP:Ce). The slower decay components the delayed radiative recombination at $Ce^{3+}$ are due to energy migration inside the Gd sublattice, but the time profile of this process is on the order of a few hundreds of ns; thus, this slower decay is still effectively captured by the standard 1 μs shaping time in the light yield measurement, i.e., does not decrease its value. The host exciton emission disappears even at a very low Gd content, which is a sign of effective energy transfer from the host to the Gd cations. The afterglow decreases by two orders of magnitude, and all TSL-evidenced electron traps become noticeably shallower. Therefore, the Gd admixture diminishes the effect of traps in LuAP:Ce and accelerates the free-carrier transport toward the Ce emission centers.

Regarding the $Ce^{3+}$ emission center itself, we successfully model its decay kinetics in the frame of Forster–Dexter theory by accounting for the following: the reverse $Ce^{3+} \rightarrow Gd^{3+}$ energy transfer, energy migration in the Gd sublattice, and delayed radiative recombination at the $Ce^{3+}$ ions. In conclusion, we report a bandgap engineered $Lu_{0.5}Gd_{0.5}AlO_3$:Ce single crystal as an excellent heavy aluminum perovskite scintillator with high potential for application in time-of-flight techniques, e.g., TOF-PET scanners and TOF-CT X-ray imaging.

**Acknowledgements**
The authors thank Mikhail Brik for the discussion about the YAP electronic structure and clarification of his first-principles calculations on this topic. The work was partially supported by the Operational Program Research, Development and Education financed by European Structural and Investment Funds and the Czech Ministry of Education, Youth and Sports (Project No. SOLID21 CZ.02.1.01/0.0/0.0/16_019/0000760) and the Technological Agency of the Czech Republic (Project No. FW01010218).

**Author details**
[1]Institute of Physics of the Czech Academy of Sciences, Cukrovarnická 10/112, 162 00 Prague 6, Czech Republic. [2]Faculty of Mathematics and Physics, Charles University in Prague, Ke Karlovu 3, 121 16 Prague 2, Czech Republic. [3]Crytur spol. s r.o., Na Lukách 2283, 511 01 Turnov, Czech Republic. [4]Faculty of Biomedical Engineering, Czech Technical University in Prague, Náměstí Sítná 3105, 272 01 Kladno, Czech Republic

**Author contributions**
The manuscript was written through quantitatively similar contributions of all authors. All authors have given approval to the final version of the manuscript.

**Competing interests**
The authors declare no competing interests.



**Supplementary information** The online version contains supplementary material available at https://doi.org/10.1038/s41427-021-00332-w.

Received: 28 June 2021 Revised: 17 August 2021 Accepted: 26 August 2021.
Published online: 22 October 2021

**References**

1. Lecoq, P., Gektin, A. & Korzhik, M. *Inorganic Scintillators for Detector Systems* (Springer, 2017).
2. Nikl, M. & Yoshikawa, A. Recent R&D trends in inorganic single-crystal scintillator materials for radiation detection. *Adv. Opt. Mater.* **3**, 463–481 (2015).
3. Weber, M. J. Nonradiative decay from 5d states of rare earths in crystals. *Solid State Commun.* **12**, 741–744 (1973).
4. Autrata, R., Schauer, P., Kvapil, J. & Kvapil, J. A single crystal of YAG-new fast scintillator in SEM. *J. Phys. E.* **11**, 707–708 (1978).
5. Nikl, M. et al. Development of LuAG-based scintillator crystals - A review. *Prog. Cryst. Growth Charact. Mater.* **59**, 47–72 (2013).
6. Kučera, M., Nikl, M., Hanuš, M. & Onderišinová, Z. Gd3+ to Ce3+ energy transfer in multi-component GdLuAG and GdYAG garnet scintillators. *Phys. Status Solidi - Rapid Res. Lett.* **7**, 571–574 (2013).
7. Bosze, E. J., Hirata, G. A., Shea-Rohwer, L. E. & McKittrick, J. M. Improving the efficiency of a blue-emitting phosphor by an energy transfer from Gd3+ to Ce3+. *J. Lumin.* **104**, 47–54 (2003).
8. Průša, P. et al. Tailoring and optimization of LuAG:Ce epitaxial film scintillation properties by Mg Co-doping. *Cryst. Growth Des.* **18**, 4998–5007 (2018).
9. Fasoli, M. et al. Band-gap engineering for removing shallow traps in rare-earth Lu3Al5O12 garnet scintillators using Ga3 + doping. *Phys. Rev. B - Condens. Matter Mater. Phys.* **84**, 1–4 (2011).
10. Nikl, M. et al. Defect engineering in Ce-doped aluminum garnet single crystal scintillators. *Cryst. Growth Des.* **14**, 4827–4833 (2014).
11. Cooke, D. W. et al. Crystal growth and optical characterization of cerium-doped Lu1.8Y0.2SiO5. *J. Appl. Phys.* https://doi.org/10.1063/1.1328775 (2000).
12. Sidletskiy, O. et al. Structure − Property correlations in a Ce-doped (Lu,Gd) 2SiO5:Ce scintillator. *Cryst. Growth Des.* **12**, 4411–4416 (2012).
13. Blahuta, S., Viana, B. & Dorenbos, P. Evidence and consequences of Ce4+ in LYSO:Ce,Ca and LYSO:Ce,Mg single crystals for medical imaging applications. *IEEE Trans. Nucl. Sci.* **60**, 3134 (2013).
14. Suzuki, A. et al. Fast and high-energy-resolution oxide scintillator: Ce-doped (La,Gd)2Si2O7. *Appl. Phys. Express* **5**, 102601 (2012).
15. Lempicki, A. et al. LuAlO3:Ce and other aluminate scintillators. *IEEE Trans. Nucl. Sci.* **42**, 280–284 (1995).
16. Lempicki, A. & Glodo, J. Ce-doped scintillators: LSO and LuAP. *Nucl. Instrum. Methods Phys. Res. Sect. A Accel. Spectrometers, Detect. Assoc. Equip.* **416**, 333–344 (1998).
17. Glodo, J. & Wojtowicz, A. J. Charge traps and emission kinetics in LuAP:Ce. *Int. Conf. Solid State Cryst. 2000 Growth, Charact. Appl. Single Cryst.* **4412**, 216–220 (2001).
18. Trummer, J., Auffray, E., Lecoq, P., Petrosyan, A. & Sempere-Roldan, P. Comparison of LuAP and LuYAP crystal properties from statistically significant batches produced with two different growth methods. *Nucl. Instrum. Methods Phys. Res. Sect. A Accel. Spectrometers, Detect. Assoc. Equip.* **551**, 339–351 (2005).
19. Korzhik, M. et al. Timing properties of Ce-doped YAP and LuYAP scintillation crystals. *Nucl. Instrum. Methods Phys. Res. Sect. A Accel. Spectrometers, Detect. Assoc. Equip.* **927**, 169–173 (2019).
20. Wojtowicz, A. J., Szupryczynski, P., Wisniewski, D., Glodo, J. & Drozdowski, W. Electron traps and scintillation mechanism in LuAlO3:Ce. *J. Phys. Condens. Matter* **13**, 9599–9619 (2001).
21. Wojtowicz, A. J. et al. Thermoluminescence and scintillation of LuAlO3:Ce. *Radiat. Meas.* **29**, 323–326 (1998).
22. Dieke, G. H., Crosswhite, H. M. & Dunn, B. Emission spectra of the doubly and triply ionized rare earths. *J. Opt. Soc. Am.* **51**, 820 (1961).
23. Mareš, J. A. et al. Further results on GdAlO3:Ce scintillator. *Radiat. Eff. Defects Solids* **135**, 369–373 (1995).
24. Dorenbos, P., Bougrine, E., De Haas, J., Van Eijk, C. W. E. & Korzhik, M. Scintillation properties of GdAlO3:Ce crystals. *Radiat. Eff. Defects Solids* **135**, 321–323 (1995).
25. Mareš, J. A., Kvapil, J., Giba, J. & Blažek, K. Spectroscopy and transfer processes in LuxGd1-xAlO3:Ce scintillators. *J. Lumin.* **72–74**, 737–739 (1997).
26. Luo, H., Bos, A. J. J. & Dorenbos, P. Controlled electron-hole trapping and detrapping process in GdAlO3 by valence band engineering. *J. Phys. Chem. C.* **120**, 5916–5925 (2016).
27. Riva, F. et al. Epitaxial growth of gadolinium and lutetium-based aluminum perovskite thin films for X-ray micro-imaging applications. *CrystEngComm* **18**, 608–615 (2016).
28. Rathaiah, M. et al. Epitaxial growth, photoluminescence and scintillation properties of Gd3+ co-doped YAlO3:Ce3+ films. *Radiat. Meas.* **121**, 86–90 (2019).
29. Zorenko, Y. V. et al. Intrinsic luminescence of YAlO3 perovskites. *Phys. Status Solidi Curr. Top. Solid State Phys.* **4**, 963–967 (2007).
30. Inokuti, M. & Hirayama, F. Influence of energy transfer by the exchange mechanism on donor luminescence. *J. Chem. Phys.* **43**, 1978–1989 (1965).
31. Kučera, M., Rathaiah, M., Beitlerová, A., Kučerková, R. & Nikl, M. Scintillation properties and energy transfer in (GdY)AlO3:Ce3+perovskites with high Gd content. *IEEE Trans. Nucl. Sci.* **67**, 1049–1054 (2020).
32. Liu, X., Pilania, G., Talapatra, A. A., Stanek, C. R. & Uberuaga, B. P. Band-edge engineering to eliminate radiation-induced defect states in perovskite scintillators. *ACS Appl. Mater. Interfaces* **12**, 46296–46305 (2020).
33. Brůža, P. et al. Applications of a table-top time-resolved luminescence spectrometer with nanosecond soft X-ray pulse excitation. *IEEE Trans. Nucl. Sci.* **61**, 448–451 (2014).
34. Dujardin, C. et al. Luminescence properties and scintillation mechanisms of cerium- and praseodymium-doped lutetium orthoaluminate. *J. Phys. Condens. Matter* **9**, 5229–5243 (1997).
35. Mihóková, E., Nikl, M., Bacci, M., Dušek, M. & Petříček, V. Assignment of 4f-5d absorption bands in Ce-doped R AlO3 (R = La, Gd, Y, Lu) perovskites. *Phys. Rev. B - Condens. Matter Mater. Phys.* **79**, 1–7 (2009).

36. Peijzel, P. S., Schrama, W. J. M. & Meijerink, A. Thulium as a sensitizer for the Gd3+/Eu3+ quantum cutting couple. *Mol. Phys.* **102**, 1285–1290 (2004).
37. Belsky, A. N. et al. Progress in the development of $LuAlO_3$-based scintillators. *IEEE Trans. Nucl. Sci.* **48**, 1095–1100 (2001).
38. Auffray, E. et al. A comprehensive and systematic study of coincidence time resolution and light yield using scintillators of different size and wrapping. *IEEE Trans. Nucl. Sci.* **60**, 3163–3171 (2013).
39. Fasoli, M. et al. Shallow traps in YAlO3: Ce single crystal perovskites. *IEEE Trans. Nucl. Sci.* **55**, 1114–1117 (2008).
40. Brik, M. G., Ma, C. G., Piasecki, M. & Suchocki, A. Locating impurity and defect levels in the host band gap by first-principles calculations: pure and Ce3+-doped YAlO3. *Opt. Mater.* **113**, 1–5 (2021).
41. Laguta, V. et al. Hole and electron traps in the YAlO3 single crystal scintillator. *Phys. Rev. B* **80**, 045114 (2009).